BRNO UNIVERSITY OF TECHNOLOGY
VYSOKÉ UČENÍ TECHNICKÉ V BRNĚ

FACULTY OF MECHANICAL ENGINEERING
FAKULTA STROJNÍHO INŽENÝRSTVÍ

INSTITUTE OF PHYSICAL ENGINEERING
ÚSTAV FYZIKÁLNÍHO INŽENÝRSTVÍ

DETECTION OF BIOCHEMICAL SUBSTANCE USING GRAPHENE SENSOR
DETEKCE BIOCHEMICKÝCH LÁTEK POMOCÍ GRAFENOVÉHO SENZORU

BACHELOR'S THESIS
BAKALÁŘSKÁ PRÁCE

AUTHOR — **Linda Supalová**
AUTOR PRÁCE

SUPERVISOR — **doc. Ing. Miroslav Bartošík, Ph.D.**
VEDOUCÍ PRÁCE

BRNO 2021

BRNO UNIVERSITY OF TECHNOLOGY
FACULTY OF MECHANICAL ENGINEERING

Assignment Bachelor's Thesis

Institut:	Institute of Physical Engineering
Student:	**Linda Supalová**
Degree programm:	Applied Sciences in Engineering
Branch:	Physical Engineering and Nanotechnology
Supervisor:	**doc. Ing. Miroslav Bartošík, Ph.D.**
Academic year:	2020/21

As provided for by the Act No. 111/98 Coll. on higher education institutions and the BUT Study and Examination Regulations, the director of the Institute hereby assigns the following topic of Bachelor's Thesis:

Detection of biochemical substance using graphene sensor

Brief Description:

Graphene has properties suitable for utilization in biosensors, e. g. high mobility of charge carriers, ultra–sensitivity of electronic properties on individual adsorbed atoms (molecules), the possibility of changing the type of charge carriers by gate voltage in a field effect transistor (FET) arrangement and as a carbon allotrope it is also compatible with biological compounds . The aim of this work is to test the electronic response of graphene to organic substances based on carbonic acid diamide and deoxyribonucleic/ribonucleic acid (DNA / RNA). In doing so, the response to different concentrations of these substances and different ways of transport response measurement in the FET arrangement with the lower solid–state and upper electrolytic gates will be mapped .

Bachelor's Thesis goals:

1. Literature search of the mentioned problem with emphasis on the possibility of detection of the mentioned compounds by means of non–functionalized graphene.
2. Measure the electronic response to different concentrations of:
a. Carbonic acid diamide (urea) and
b. DNA / RNA based substances.
3. Measure the resistance response in different electronic connections of the FET–based graphene biosensor, e.g.
a. without gate,
b. with an upper electrolytic gate and
c. with a lower solid–state gate.
4. Analyze and discuss the results obtained by individual methods of measurement and compare with similar results in the literature.

Recommended bibliography:

CASTRO NETO, A. H., F. GUINEA, N. M. R. PERES, K. S. NOVOSELOV a A. K. GEIM. The electronic properties of graphene. Reviews of Modern Physics. 2009, 81(1), 109-162. ISSN 0034-6861. Dostupné z: doi:10.1103/RevModPhys.81.109

SCHEDIN, F., A. K. GEIM, S. V. MOROZOV, E. W. HILL, P. BLAKE, M. I. KATSNELSON a K. S. NOVOSELOV. Detection of individual gas molecules adsorbed on graphene. Nature Materials. 2007, 6(9), 652-655. ISSN 1476-1122. Dostupné z: doi:10.1038/nmat1967

HWANG, Michael Taeyoung, Mohammad HEIRANIAN, Yerim KIM, et al. Ultrasensitive detection of nucleic acids using deformed graphene channel field effect biosensors. Nature Communications. 2020, 11(1), 1543. ISSN 2041-1723. Dostupné z: doi:10.1038/s41467-020-15330-9

BARTOŠÍK, Miroslav, Jindřich MACH, Jakub PIASTEK, David NEZVAL, Martin KONEČNÝ, Vojtěch ŠVARC, Klaus ENSSLIN a Tomáš ŠIKOLA. Mechanism and Suppression of Physisorbed-Wate--Caused Hysteresis in Graphene FET Sensors. ACS Sensors. 2020, 5(9), 2940-2949. ISSN 2379-3694. Dostupné z: doi:10.1021/acssensors.0c01441

TRIPSKÝ, Andrej. Design, fabrication and testing of graphene biosensors. Brno, 2020. Diplomová práce. Vysoké učení technické v Brně, Fakulta strojního inženýrství, Ústav fyzikálního inženýrství.

Deadline for submission Bachelor's Thesis is given by the Schedule of the Academic year 2020/21

In Brno,

L. S.

prof. RNDr. Tomáš Šikola, CSc.
Director of the Institute

doc. Ing. Jaroslav Katolický, Ph.D.
FME dean

ABSTRACT

This bachelor's thesis aims to study the interaction of biochemical substances with graphene by utilizing sensors with a field-effect transistor arrangement. Adsorbed atoms or molecules can induce doping of the graphene sheet, which can be experimentally determined by observing the shift in the position of the Dirac point. Dependence of the Dirac point position on the added substance is studied, as well as time response to the addition of the liquid sample. Sensitivity to different molecules is observed and the implication of the results for the adsorption of various molecules are discussed.

KEYWORDS

graphene, sensor, fielf-effect transistor, adsorption, urea, nucleic acids, Dirac point

ABSTRAKT

Tato bakalářská práce studuje interakci biochemických látek s grafénem pomocí senzorů v uspořádání polem řízeného tranzistoru. Adsorbované atomy nebo molekuly mohou vyvolat dopování grafénové vrstvy, což může být experimentálně určeno pozorováním změny pozice Diracova bodu. Je studována závislost polohy Diracova bodu na přidané látce a stejně tak i časová odezva na přidání kapalného vzorku. Je pozorována citlivost na odlišné molekuly a jsou dikutovány důsledky výsledků pro adsorpci různých molekul.

KLÍČOVÁ SLOVA

grafén, senzor, polem řízený tranzistor, adsorpce, močovina, nukleové kyseliny, Diracův bod

SUPALOVÁ, Linda. *Detection of biochemical substance using graphene sensor*. Brno, 2021, 52 p. Bachelor's Thesis. Brno University of Technology, Faculty of Mechanical Engineering, Institute of Physical Engineering. Advised by doc. Ing. Miroslav Bartošík, Ph.D.

DECLARATION

I declare that I have written the Bachelor's Thesis titled "Detection of biochemical substance using graphene sensor" independently, under the guidance of the advisor and using exclusively the technical references and other sources of information cited in the thesis and listed in the comprehensive bibliography at the end of the thesis.

As the author I furthermore declare that, with respect to the creation of this Bachelor's Thesis, I have not infringed any copyright or violated anyone's personal and/or ownership rights. In this context, I am fully aware of the consequences of breaking Regulation § 11 of the Copyright Act No. 121/2000 Coll. of the Czech Republic, as amended, and of any breach of rights related to intellectual property or introduced within amendments to relevant Acts such as the Intellectual Property Act or the Criminal Code, Act No. 40/2009 Coll., Section 2, Head VI, Part 4.

Brno ....

author's signature

ACKNOWLEDGEMENT

I want to acknowledge the assistance of my supervisor doc. Ing. Miroslav Bartošík, Ph.D., in providing the theoretical background needed for the interpretation of results. The experimental part of this work would not be possible without all the support from Ing. Jakub Piastek and Ing. Vojtěch Švarc. I cannot appreciate enough their experience in fabrication of graphene-based devices and the setup of the experiments, as well as their moral support. A special thanks to my classmate, Lukáš Zezulka, always willing to provide motivation during writing of this thesis and ready to share our common grievances.

Contents

Introduction

Since its discovery in 2004 [1], graphene has taken the world of scientific research by storm. The potential of this novel material has been explored in applications ranging from composite materials and anti-corrosive coatings to energy storage and biomedical diagnostics.

The unique electronic properties of graphene, such as high carrier mobility and ambipolar field effect, combined with an extremely high surface-to-volume ratio allow for sensors based on field-effect transistors to achieve extraordinarily low limits of detection. These sensors offer considerable promise in various fields, including monitoring of environmental pollutants, early medical diagnostics, and DNA sequencing.

However, selective sensing of substances requires functionalization of graphene and the first step in this direction is understanding the mechanism of adsorption of biological molecules on non-functionalized graphene. For this purpose, three different molecules based on nucleic acids are studied.

Additionally, the detection of urea by a graphene sensor is examined in this thesis. Urea solution has found its use as an additive in diesel motors to lower NO_x emissions and graphene sensors placed in these motors could monitor the concentration of urea, assessing whether, e.g., water was used instead.

The theoretical part of this work introduces graphene and the working principles of sensors in the FET arrangement, along with the state of the art of biosensing capabilities of graphene sensors. In the experimental part, two designs of graphene sensors are fabricated and two types of experiments are performed to investigate the interaction of graphene with the measured biochemical substances. Finally, the results obtained from these experiments are presented and discussed.

1 Graphene

Graphene is a two-dimensional allotrope of carbon with the atoms arranged in a hexagonal (honeycomb) lattice, Fig. 1.1, where the individual carbon atoms are spaced 1.42 Å apart. This novel material was first isolated by Geim and Novoselov in 2004 [1], although the structure had been used as a theoretical model for various calculations in graphite decades prior.

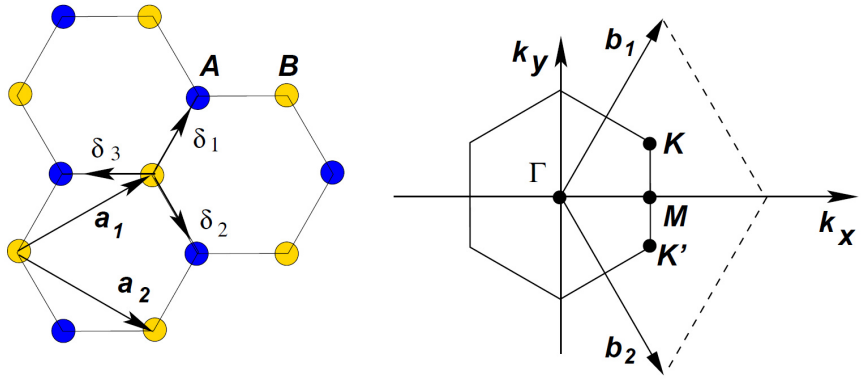

Fig. 1.1: The lattice of graphene in real (left) and reciprocal space (right). a_i denote lattice primitive vectors, δ_i are the nearest neighbour vectors, and b_i are the reciprocal lattice vectors. Points K and K' on the edge of the Brillouin zone are called the Dirac points. Adapted from [6].

Carbon atoms form strong covalent sp^2 bonds in the plane of the graphene monolayer with π-orbitals perpendicular to it. This arrangement is responsible for some of the unique electronic properties of graphene, as will be discussed in detail later. Another important consequence of the structure is the resistance to in-plane deformations characterized by high Young modulus $E = 1\,\mathrm{TPa}$ [2] for defect-free graphene. Other interesting properties of graphene for different applications include high in-plane thermal conductivity of $5000\,\mathrm{WmK^{-1}}$ [3] for thermal management in electronics, light transmittance $\sim 97.7\,\%$ [4] useful in optoelectronics, or gas impermeability [5] that makes graphene a possible candidate for anti-corrosive coatings.

1.1 Electronic properties

Graphene is often described as a zero band gap semiconductor due to the band structure and the subsequent behavior of charge carriers at the Dirac points K and K'. The charge carriers (called Dirac fermions) behave as relativistic particles with zero rest mass moving at the Fermi speed $v_\mathrm{F} \approx 10^6\,\mathrm{m/s}$ in these points and can be

continuously converted from electrons to holes (and vice versa) by the application of an external electric field, which makes graphene predisposed for use in electronics.

The dispersion relation forms valence and conduction bands as cones that meet in exactly one point, Fig. 1.2. When the *Fermi level* (E_F) intersects this point, the conductivity of graphene is at its lowest, as the number of holes and electrons is in equilibrium.

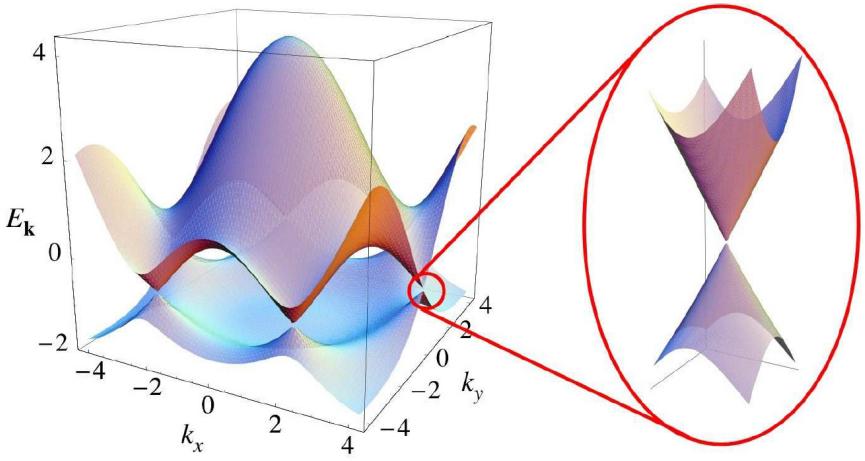

Fig. 1.2: Energy spectrum of graphene dependent on the wave vectors with a zoom-in on the energy bands at one of the Dirac points. Adapted from [6].

This balanced state of charge carriers is true only for pristine graphene, but real graphene samples are highly susceptible to doping of both p and n type, which consequently changes the Fermi level. Adsorption of atoms or molecules on the surface can cause electrostatic doping, which is studied in this thesis.

1.2 Preparation by CVD

There are several possible ways of graphene fabrication (e.g., mechanical exfoliation, epitaxial growth, and thermal decomposition of SiC), but *chemical vapour deposition* (CVD) is the most promising method for large-scale, commercial production. In CVD, a precursor gas is injected into the chamber, which reacts with or thermally decomposes on a substrate.

For graphene preparation, methane or ethylene are most commonly used as precursor gases that break down into carbon and hydrogen atoms, but almost any organic substance containing carbon can be used [7]. Common substrates include copper and nickel, but copper foil is preferred due to the low solubility of carbon in copper compared to nickel, therefore carbon atoms precipitate on the substrate surface instead of first diffusing into the substrate bulk.

The exact growth parameters differ depending on the precursor gas, the substrate, and the CVD furnace construction, among others. Using copper foil as the substrate, the first step is annealing at high temperature (approximately 1000 °C) in argon to smooth out the substrate surface before heating in H_2 atmosphere at low pressure. In the next phase, methane is added into the chamber, where the molecules decompose. Hydrogen atoms are removed away by continuous H_2 gas flow, while carbon atoms accumulate on the substrate and create growth centers that expand into grains. These grains increase in size until they connect with neighbouring grains and form a monolayer of graphene. The growth stops once the whole copper foil is covered, but multilayers can emerge in the places of the original growth centers if the growth rate is too quick. In this case, the second and third layers begin forming before the whole foil is covered with the graphene monolayer.

2 Graphene sensors based on field-effect transistors

Due to its unique structure and electronic properties, graphene is a promising candidate for all manner of sensors. Shedin et al. developed a graphene sensor able to detect individual gas molecules [9]. Selective detection of nucleic acids on functionalized graphene with the *limit of detection* (LOD) in the order of pM was also observed [10]. One type of sensor design that stands out because of its fast response and relatively simple test procedure is a *field-effect transistor* (FET). Additionally, FET sensors have inherently high sensitivity and low LOD due to the amplifying function of transistors.

The classical FET consists of three electrodes (source, drain, and gate), a semiconducting channel between source and drain, and an insulating layer that separates the channel from gate. At a constant voltage V_{SD} between source and drain, the current I_{SD} flowing through the channel can be modulated by the *gate voltage* (V_{G}).

In the case of *graphene field-effect transistor* (GFET), graphene serves as the conductive channel that is able to utilize both holes and electrons as charge carriers depending on the applied gate voltage due to its ambipolar character. Fig. 2.1 shows the typical transfer curve for a GFET with the peak of the $R(V_G)$ dependency corresponding to the so-called *Dirac point voltage* (V_{D}), where the charge carriers are in equilibrium.

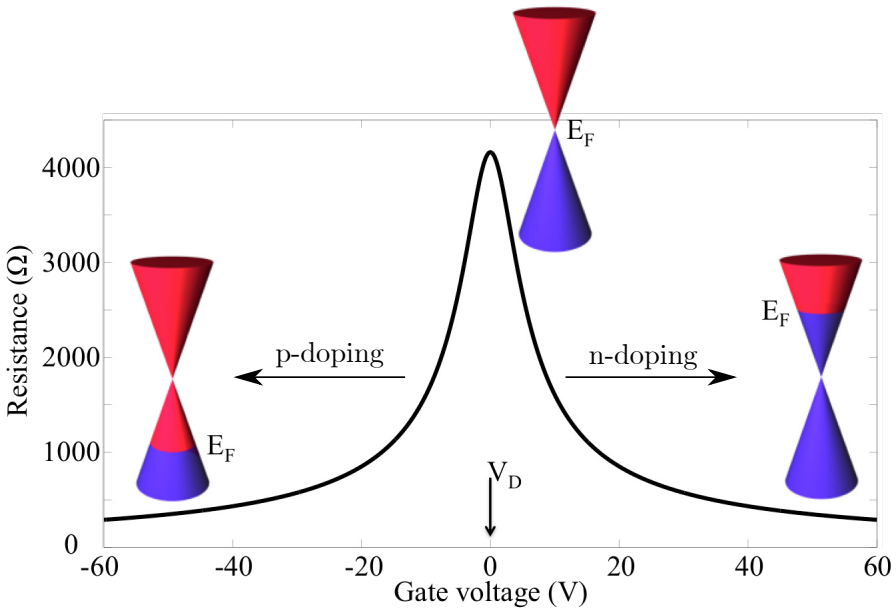

Fig. 2.1: Dependency of resistance R on applied gate voltage V_{G}. Adapted from [11].

2.1 Bottom-gated FET sensors

A traditional FET has a solid-state bottom gate (Fig. 2.2), analogously a silicon substrate is usually used as the bottom gate for a GFET with a thin layer of *silicon dioxide* (SiO_2) as the insulator. The conductivity of the graphene channel is modulated directly by applying gate voltage V_G.

Using the model of a parallel-plate capacitor, the concentration of the majority carriers in graphene can be calculated from V_{G}. The capacitance of a capacitor is defined as the ratio of charge and voltage:

$$C = \frac{Q}{V}. \tag{2.1}$$

For a parallel-plate capacitor, the capacitance can be calculated as [12]:

$$C = \frac{\varepsilon_0 \varepsilon_{\mathrm{r}} A}{d}, \tag{2.2}$$

where ε_0 is the permittivity of vacuum, ε_{r} the relative permittivity of the dielectric, A the area of the plates and d the distance between them. For GFET, the dielectric is the SiO_2 layer and the charge Q can be expressed as the elementary charge e multiplied by the number of majority carriers N in graphene. After substituting $Q = Ne$ and combining equations 2.1 and 2.2:

$$N = \frac{\varepsilon_0 \varepsilon_{\mathrm{r}} A}{ed} V. \tag{2.3}$$

Considering that graphene is a 2D structure, the concentration of majority carriers n depending on the gate voltage V_{G} can be determined as:

$$n = \frac{N}{A} = \frac{\varepsilon_0 \varepsilon_{\mathrm{r}}}{ed} V_G. \tag{2.4}$$

2.2 Top-gated FET sensors

Another way of insulating the channel from the gate electrode is to apply a high-resistive electrolytic solution on the channel and add a top gate from above (Fig. 2.2). In this case, an *electric double layer* (EDL) forms at the graphene/electrolyte interface. Some ions in the electrolyte are immobilized on the graphene surface, while the rest of them creates a diffuse layer. The thickness of EDL, called the *Debye length* (λ_{D}), depends on the ionic strength I of the electrolyte as [13]:

$$\lambda_{\mathrm{D}} = \sqrt{\frac{\varepsilon_0 \varepsilon_{\mathrm{r}} k_{\mathrm{B}} T}{2 N_{\mathrm{A}} e^2 I}}, \tag{2.5}$$

where ε_{r} represents the relative permittivity of the electrolyte, k_{B} the Boltzmann constant, T the temperature, and N_{A} the Avogadro constant.

Any ions at a distance further from the graphene surface than λ_D are screened by the EDL, which prevents them from interacting with graphene. Therefore, a large Debye length in the electrolyte is always desirable to heighten the sensitivity by increasing the distance at which analytes can influence graphene. But it is also an essential requirement for graphene functionalized by probe molecules adsorbed on the surface, because the height of the probes themselves needs to be taken under consideration.

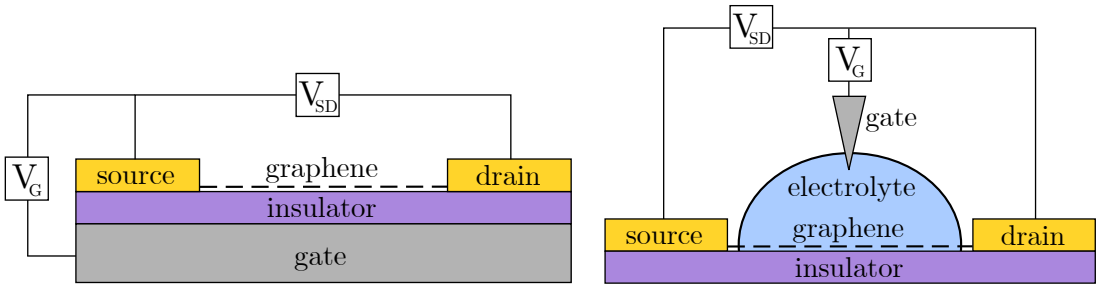

Fig. 2.2: Schematic of a bottom-gated (left) and a top-gated (right) GFET.

Electrolyte-gated GFETs are especially suitable for use as biosensors due to low operating potentials (usually in the range of $\pm 1\,\mathrm{V}$), that prevent redox reactions and splitting of molecules.

2.3 The sensing mechanism

A molecule adsorbed on graphene modulates its conductivity by changing the Fermi level E_F. For example, the adsorption of a water molecule (an electron acceptor) would lower the E_F under the Dirac point, resulting in the p-doping of graphene, which is reflected in the shift of the transfer curve to the right compared to pristine graphene.

Applying positive V_G on bottom electrode increases the concentration of electrons leading to the rise of E_F. In the case of originally p-doped graphene, it corresponds to the increase in the resistance of graphene as the concentration of holes (the majority carriers) decreases. The transfer curve reaches its peak as E_F intersects Dirac point and there is no predominant doping of p or n type to enhance the conductivity of graphene. Additional increase of V_G moves E_F further above the Dirac point and the resistance decreases as electrons become the majority carriers and their concentration increases with the application of positive V_G.

To compare the doping effect of different molecules, either the shift of the transfer curve or the concentration of majority carriers n at the Dirac voltage V_{D} (calculated from eq. 2.4) are used.

3 Interactions of biomolecules and graphene

In general, there are two main effects at play when biomolecules interact with graphene: non-covalent $\pi - \pi$ stacking and molecular doping.

Many organic molecules contain aromatic rings with delocalized π-electrons and the same delocalization of electrons is observed in graphene due to the sp^2 hybridization of carbon atoms. To model the interactions between such π-systems, it is convenient to simplify the molecules by dividing them into a positive planar framework and a negative cloud of π-electrons above and below, as suggested by Hunter and Sanders in [14]. The π-electrons roughly copy the shape of the aromatic ring with an electron-poor region in the middle.

In the presented model, the geometry of the $\pi - \pi$ interaction is dictated by electrostatic interaction and the strength of the $\pi - \pi$ interaction is controlled by van der Waals forces. The π-electrons of different π-systems repulse each other and force the molecules to adopt a geometric arrangement that minimizes this repulsion, while maximizing the attraction between the π-electrons of one molecule and the positive framework in the electron-poor cavity of the other molecule. This can create a major offset in the positioning of the two π-system on top of each other, see Fig. 3.1. The alignment of the molecules depends on the distribution of electron-rich and electron-poor regions rather than on the overall molecular potential.

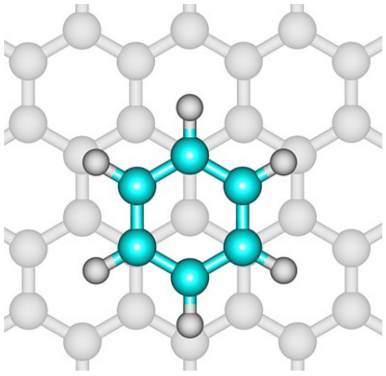

Fig. 3.1: Offset geometry illustrated on the adsorption of benzene on top of graphene. Adapted from [15]

The van der Waals forces contribute to the energy of the interaction and are roughly proportional to the overlap area of the π-electron clouds of the molecules. The magnitude of the interaction can be critically influenced by atoms in the regions of intermolecular contact.

These atoms in the intermolecular region can also be directly responsible for the molecular doping of graphene. The proximity of a charged atom or molecular region close to the graphene surface results in charge transfer and doping of graphene.

3.1 Nucleic acids

Nucleic acids form the foundation of all living organisms. *Deoxyribonucleic acid* (DNA) stores the information necessary for the synthesis of proteins, while *ribonucleic acid* (RNA) is responsible for the transmission of this information and the protein synthesis itself [16].

Nucleic acids can be broken down into the following structural units: nucleobases, a pentose (a 5-carbon sugar), and a phosphate group.

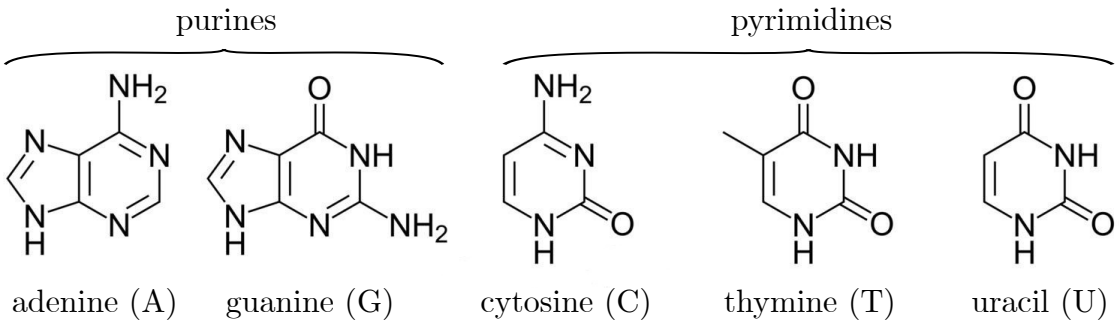

Fig. 3.2: The five primary nucleobases.

There are five primary nucleobases: adenine (A), cytosine (C), guanine (G), thymine (T), and uracil (U), which can be divided into the purine and pyrimidine groups, Fig. 3.2. Nucleobases from each group form complementary base pairs C-G and A-T that connect the two strands of the double-helical DNA structure.

Adding a pentose to a nucleobase creates a nucleoside. The pentose is either ribose or 2-deoxyribose depending on whether the molecule is found in RNA or DNA.

Substituting the 5'-OH group in the pentose with one or more phosphate groups produces a nucleotide, Fig. 3.3. The phosphate group binds to the pentose of a neighbouring nucleotide in the DNA or RNA chain, forming the so-called backbone of the single- or double-helical spiral.

The aromatic rings that comprise the nucleobases make possible the physisorption of nucleic acids on graphene by the $\pi - \pi$ stacking interaction. This has been studied both theoretically by *density functional theory* (DFT) calculations [17, 18, 19] and experimentally [20, 21]. In the case of nucleobases and nucleosides, n-doping of graphene and the subsequent increase in the Fermi level are observed. The effect of the adsorption of nucleotides depends heavily on the positioning of the molecule on top of graphene due to the negatively charged phosphate group that can cause molecular p-doping of graphene when in close proximity to the sheet.

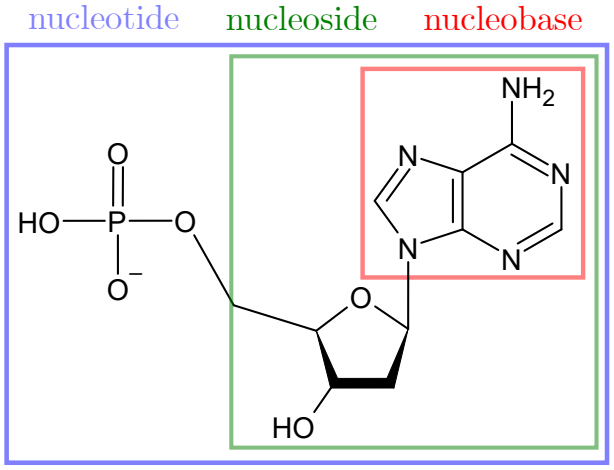

Fig. 3.3: Composition of a nucleotide, which is comprised of a nucleoside and one or more phosphate groups.

3.2 Urea

Urea is an organic compound consisting of two amine groups attached to a carbonyl group, NH_2-CO-NH_2. Low and high levels of urea in blood and urine are indicative of various health problems concerning mainly kidneys and liver. Urea is also widely used as a fertilizer in agriculture, but it decomposes into toxic ammonia, an environmental pollutant. Urea solution is utilized as an additive in diesel motors to lower NO_x emissions. Therefore, the accurate detection of urea and the estimate of concentration are of great importance in many areas, including healthcare, agriculture, and environmental monitoring.

Based on a theoretical study [22] done using DFT calculations, it is predicted that urea interacts very weakly with pristine graphene. The high distance between the molecule and graphene of 2.86 Å, the low adsorption energy of $E_{\text{ads}} = -0.776\,\text{eV}$, and no observed changes at the Fermi level in *density of states* (DOS) all indicate that only weak chemisorption occurs. This is further supported by the fact that the calculated charge transfer is only 0.065 e from the graphene layer to the urea molecule, resulting in a small p-doping of graphene. The same study also investigates the effect of doping graphene with transition metal atoms and proposes this functionalization of graphene to improve the adsorption of organic compounds.

4 Sensor fabrication

The whole process of sensor preparation takes place at the Central European Institute for Technology (CEITEC).

4.1 Methods used for the preparation of sensors

4.1.1 Optical lithography

Optical lithography is used for the fabrication of structures on the sample surface using a beam of focused (usually ultra-violet-UV) light and resist (a substance that changes its structure upon interaction with light). Generally, resists are labeled as either positive, or negative depending on whether the exposure to UV light strengthens (negative ones) or weakens the resist structure (positive ones). Chemical processes then remove the weaker parts of the structure, i. e., the exposed parts are removed with the use of a positive resist, while with a negative resist the non-exposed areas removed.

Optical lithography enables the preparation of multiple samples at the same time, however, the lower limit for the size of the structures is 1 μm.

4.1.2 Electron-beam physical vapour deposition

Physical vapour deposition (PVD) is a method used to create thin films and coatings. For *electron-beam physical vapour deposition* (EBPVD) is the source material in the form of pellets in a crucible heated by a focused electron beam. Under *ultra high vacuum* (UHV) conditions, the heated material evaporates, the vapours then travel through the vacuum chamber and precipitate on the cooler sample surface resulting in a thin layer of the source material.

EBPVD can achieve high deposition rates with high material utilization efficiency and excellent uniformity of coating.

4.1.3 Reactive-ion etching

Reactive-ion etching (RIE) is a dry etching method and achieves very anisotropic etch profiles compared to the usually isotropic effect of wet etching. An oscillating RF field is applied to the vacuum chamber that ionizes the gas molecules. Every half of the RF cycle, the electrons hit the powered lower electrode, which then acquires a negative self-bias that attracts the ions from plasma to the sample surface. The impact of the high-energy ions causes sputtering in addition to chemical reaction with the sample materials.

4.1.4 Graphene transfer

Graphene is grown by CVD (see section 1.2) on copper foil and is transferred onto the prepatterned silicon wafer using the "wet" transfer method.

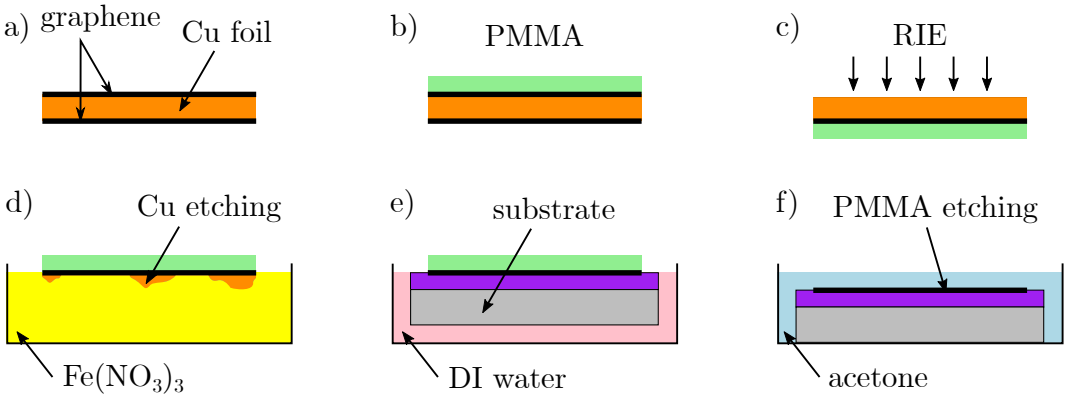

Fig. 4.1: Step-by-step schematic of the graphene transfer process. Adapted from [23].

First, graphene is grown on both sides of the copper foil in a CVD furnace, Fig. 4.1 a). Second, a thin film of *poly(methyl methacrylate)* (PMMA) is spin-coated on graphene (the liquid solution is applied onto a rotating substrate to form a thin layer) and left to dry overnight, Fig. 4.1 b). This PMMA layer acts as a support structure and prevents mechanical damage of graphene during the transfer processes. Third, the other side of the copper foil is cleaned by RIE to remove any possible residue of graphene, Fig. 4.1 c). Fourth, the copper foil beneath graphene is etched away in $Fe(NO_3)_3 \cdot 9\,H_2O$, Fig. 4.1 d). Fifth, the graphene layer with the PMMA film floats on the liquid surface and can be scooped on a prepared, clean sample and moved into a different solution. The graphene sample is moved into deionized (DI) water four times with this method, Fig. 4.1 e). To ensure that no iron residue remains from the $Fe(NO_3)_3 \cdot 9\,H_2O$ etching, the graphene layer is transferred into hydrochloric acid (HCl) for 5 minutes and then four times into DI water and at last into ethanol to remove any other contaminants. The clean graphene layer is carefully scooped on the sample surface and left to dry overnight.

The last step concerns the removal of the PMMA layer. The sample is baked for 45 minutes on a hot plate at temperatures rising from 60 °C to 105 °C to evaporate residual water and then left in acetone heated at 52 °C for 2 hours to etch the PMMA film, Fig. 4.1 f). Finally, the sample is cleaned one last time in isopropyl alcohol and ethanol and left to dry.

4.2 Sensor preparation

Previously cleaned silicon wafers with a 280 nm thick layer of SiO_2 are used as the substrate for the sensors.

The first step involves optical lithography and deposition by electron-beam evaporation (as described in sections 4.1.1 and 4.1.2) to create the gold electrodes, Fig. 4.2. The silicon wafer is spin-coated with the positive photoresist AZ 5214 E, Fig. 4.2 a), which is followed by UV light exposure, Fig. 4.2 b), and development in the AZ 726 MIF developer, Fig. 4.2 c). The prepared sample is then covered by 5 nm of Ti and an 80 nm thick layer of AU, Fig. 4.2 d). The Ti thin film ensures better adhesion of Au to SiO_2. Most of this gold layer is then removed during the so-called "lift-of" process, which leaves Au only in the designated areas that were exposed during lithography, Fig. 4.2 e).

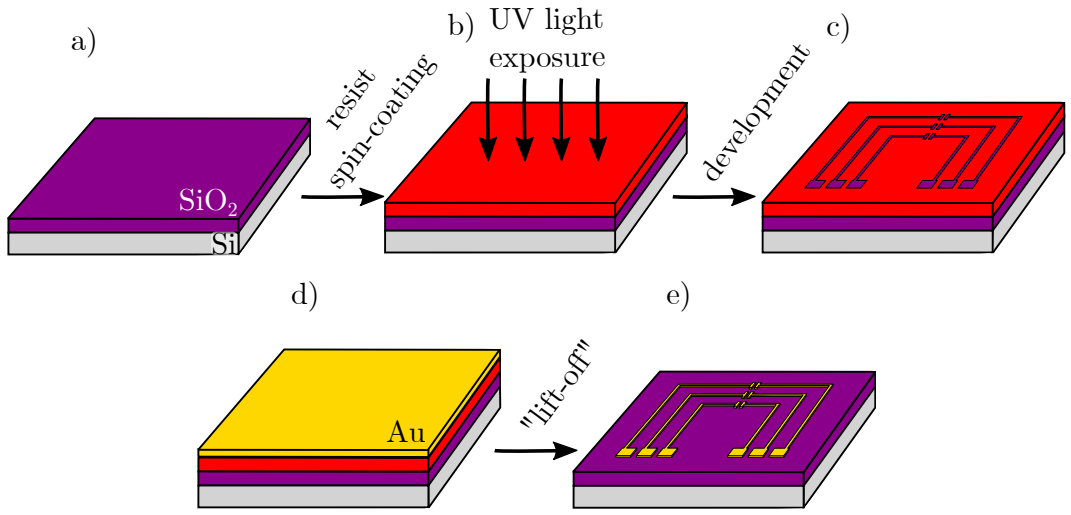

Fig. 4.2: Step-by-step schematic for the fabrication of electrodes. Adapted from [23].

This initial lithography is followed by the transfer of graphene onto the pre-patterned sample (for details see section 4.1.4). It is necessary to clean the sample by RIE just before transfering the graphene sheet to ensure that the graphene layer does not tear and that no contaminants stay between graphene and the sample surface.

The next step aims to shape the graphene layer into a Hall bar structure using optical lithography. The sample is spin-coated with a thin layer of PMMA and the negative photoresist AR-N 4340 before exposure and development in the AR 300-475 developer. The remaining resist and the graphene outside the desired Hall bar shape are removed by RIE.

Finally, the sample is baked at 180 °C for 30 minutes to ensure better adhesion of graphene to the surface, the sample is then attached by a conductive silver paint and wire-bonded onto a expander.

5 Experiments

5.1 Sensor designs

Two sensor designs are used for the measurements, Fig. 5.1. The first design utilizes Hall bar shaping of graphene, Fig. 5.1 a), and the second design uses a simpler 2-probe setup consisting of two probes fully covered by non-patterned graphene, Fig. 5.1 b). Both sensor designs are manufactured as described in section 4.2 with only one difference: the step of shaping graphene by optical lithography is left out in the case of the 2-probe samples.

During the fabrication process of these two designs, it has been proved that baking the sample after graphene transfer is crucial for the durability of the sensors. The lithographic process of shaping the Hall bars includes several short periods of baking, therefore a separate baking step before the attachment to the expander is unnecessary. Omitting this step in the case of the 2-probe samples results in tearing of graphene upon the removal of liquid from the sensor surface (both by sucking it off with a pipette or by letting it dry out in atmospheric conditions). After implementing this baking step, the 2-probe samples can last several hours of continuous measurements with only a moderate change ($\approx 10^2\,\Omega$) in the resistance of graphene (which commonly has resistance in the range of $300 - 2000\,\Omega$).

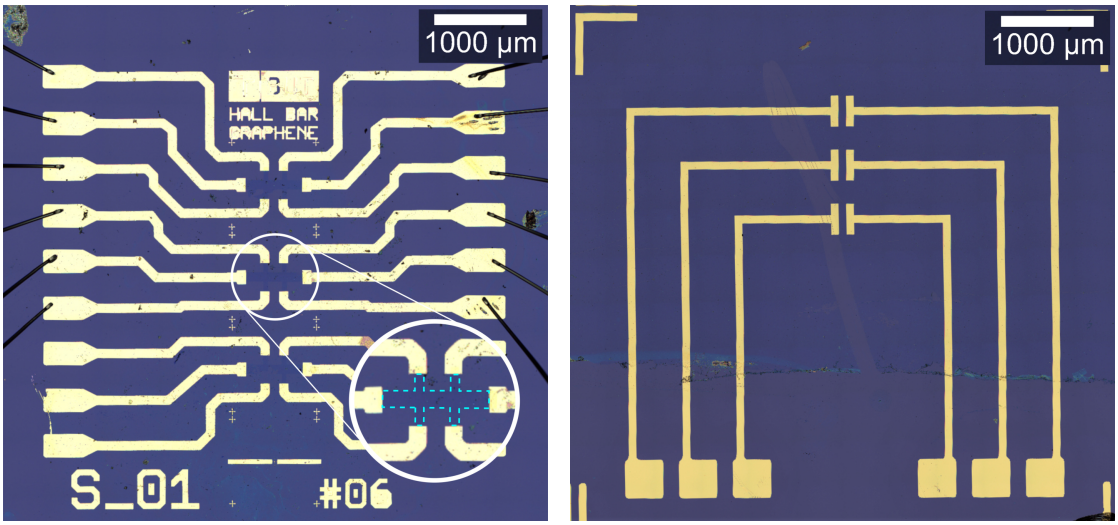

Fig. 5.1: Images of the used sensors under an optical microscope. Left: The arrangement of a sample with three Hall bars, the detail of the central Hall bar with the dashed line designating the area covered by graphene. Right: 2-probe design with graphene covering the upper part of the sample.

5.2 Characterization of the sensors by Raman spectra

Raman spectroscopy was performed at CEITEC to assess the quality of graphene on the used sensors. Raman spectra of graphene are characterized by the presence of G peak at $\sim 1600\,\mathrm{cm}^{-1}$ and 2D peak at $\sim 2700\,\mathrm{cm}^{-1}$. The G peak appears due to the sp^2 hybridization of carbon atoms in graphene. The intensity of the 2D peak determines the number of graphene layers, a ratio of 2:1 and higher of the 2D:G peaks proves that the graphene sheet is monolayer. A third peak (D) can appear at $\sim 1350\,\mathrm{cm}^{-1}$, that indicates the presence of defects in the crystal structure of graphene.

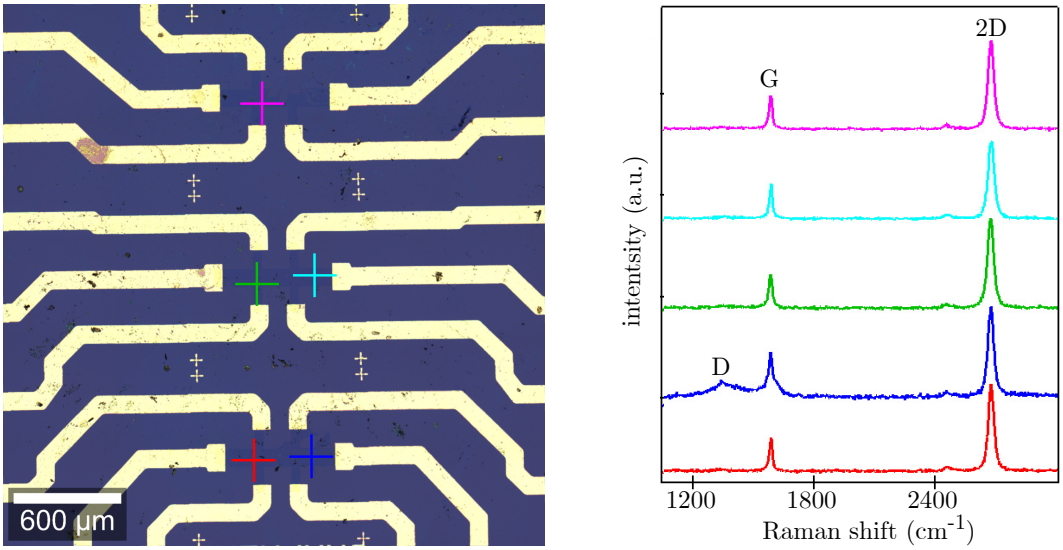

Fig. 5.2: Raman spectra of the Hall bar design in selected points.

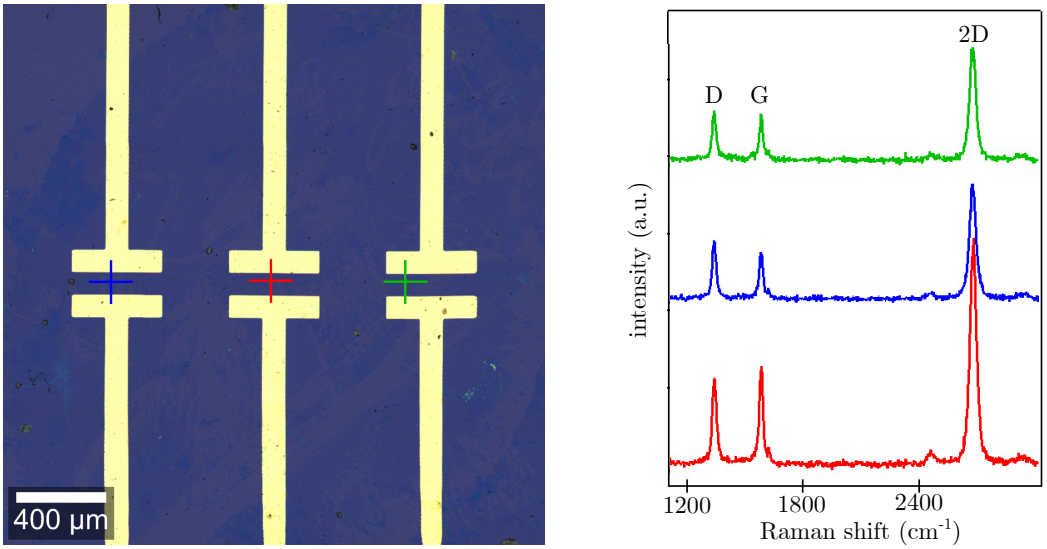

Fig. 5.3: Raman spectra of the 2-probe design in selected points.

Based on the Raman spectra of graphene on the Hall bar sensors (Fig. 5.2), the graphene sheet is monolayer and almost defectless. The graphene sheet on the 2-probe sensors (Fig. 5.3) is also monolayer, but its crystal structure contains a large number of defects as shown by the high intensity of the D peak.

5.3 Biochemical samples

The Institute of Biophysics of the Czech Academy of Sciences provided the following samples of substances based on nucleic acids (Fig. 5.4): *adenine* (A), *adenosine* (A-N), and *deoxyadenosine monophosphate* (dAMP). Both adenosine and deoxyadenosine monophosphate are based on the nucleobase adenine, therefore let us call these samples adenine-based for simplicity. All samples were prepared in concentrations of 0.1 mM, 1 mM, and 10 mM in aqueous solution.

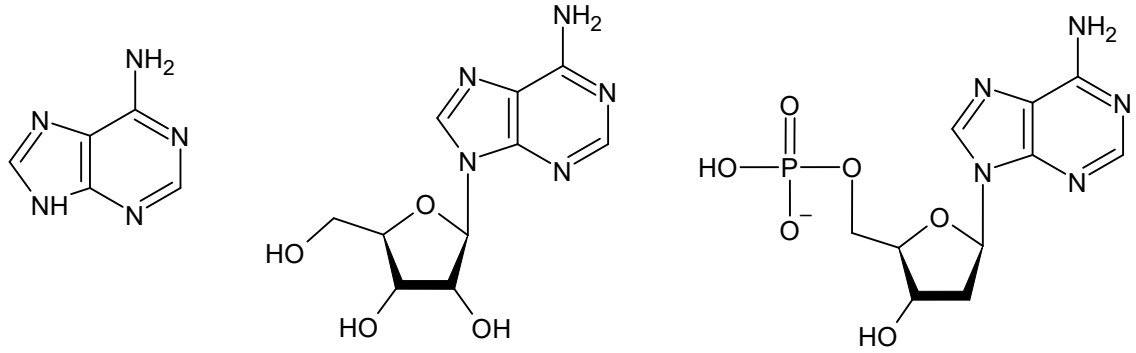

Fig. 5.4: Chemical structure of the samples (left to right): adenine, adenosine, and deoxyadenosine monophosphate.

For the samples of urea, Fig. 5.5, four concentrations (10 %, 20 %, 35 %, and 50 %) were prepared by dissolving crystalline urea in DI water.

Measurements of adenine-based samples were done on sensors with the 2-probe design. Sensors with the Hall bar shape of graphene were used for the measurements of urea.

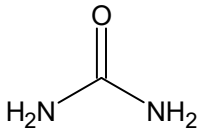

Fig. 5.5: Chemical structure of urea.

5.4 Measurements

The experimental setup (Fig. 5.6) utilizes the FET arrangement of the sensors.

The gate voltage is realized by current source connected parallel to 1 MΩ resistor. For the measurements with bottom gating, the gate electrode is connected directly to the sensor, while the electrolytic top gating is managed by applying voltage to a needle inserted from above into the droplet and without touching the graphene layer at the same time.

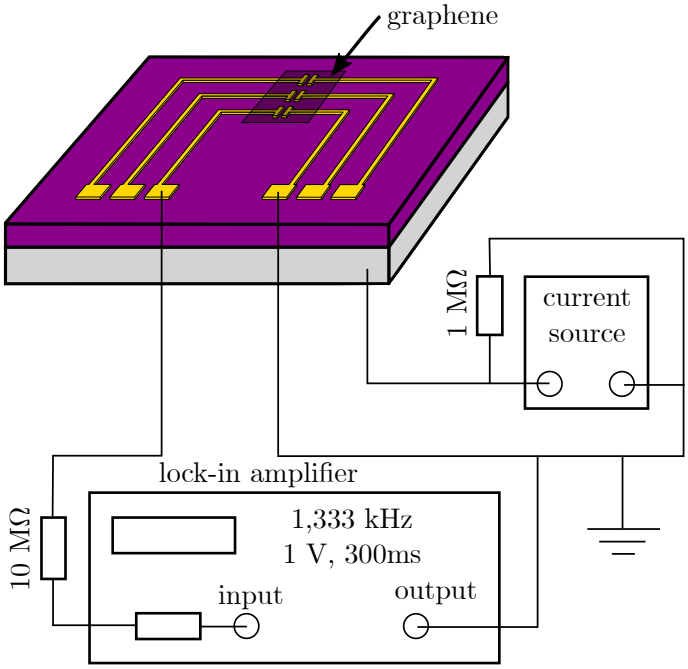

Fig. 5.6: The electrical circuit of the experimental setup. Adapted from [23].

A lock-in amplifier for resistance measurement is placed between source and drain. The signal from lock-in amplifier goes through 10 MΩ resistor before passing through the graphene layer. The voltage is set to 1 V and the 10 MΩ resistor determines the current $I_{SD} = 100\,\text{nA}$. The resistance of the examined biochemical substances was measured to be in the order of $10^0 - 10^1\,\text{M}\Omega$, therefore current leakage through the measured solution is negligible and all current flows through the graphene layer.

The individual parameters for the measurements can be adjusted in a program using LabView environment.

5.4.1 Time response

The first type of measurement examines the sensor response to the addition of different substances. The resistance as a function of time is measured without

the application of gate voltage, i.e., at $V_G = 0\,V$.

First, the sensor resistance is measured in atmospheric conditions for 30 s to obtain a mean value of the initial resistance. A droplet of the measured substance is added with a pipette on top of the graphene sheet and left there for several minutes until stabilization of the resistance is observed. Then the droplet is sucked off by pipette and the sensor surface is cleaned by adding and removing a large drop of DI water several times. Several minutes are needed for the sensor to stabilize in atmospheric conditions again.

5.4.2 Transfer curve

The second type of measurement uses either the bottom or top gate to obtain the transfer curve of graphene by tracking the change of resistance depending on the applied gate voltage.

The gate voltage is swept from 0 → maximal value → minimal value → 0. There is a significant hysteresis characterized by a shift of the whole transfer curve, that is noticeable by sweeping in both directions. Using the electrolytic top gate, the sweep is in the range of $\pm 1\,V$, however, the sweeping range for the bottom gate can reach values up to $\pm 80\,V$ if needed.

Between measurements of different substances and concentrations, the sensor surface is thoroughly cleaned with isopropyl alcohol and ethanol to remove any organic contaminants from previous experiments.

6 Results

6.1 Time response measurements

Fig. 6.1 shows the measured response in time for adenosine (A-N) without the application of gate voltage. The addition of the droplet causes a sharp increase of resistance followed by a stabilization period, when the resistance rises at a slower rate. The sudden jumps in resistance right after the removal of the droplet correspond to the cleaning of the sensor surface by pipetting on and off drops of DI water. During the stabilization in ambient conditions, the resistance decreases and returns back to the initial value measured before the application of the examined substance.

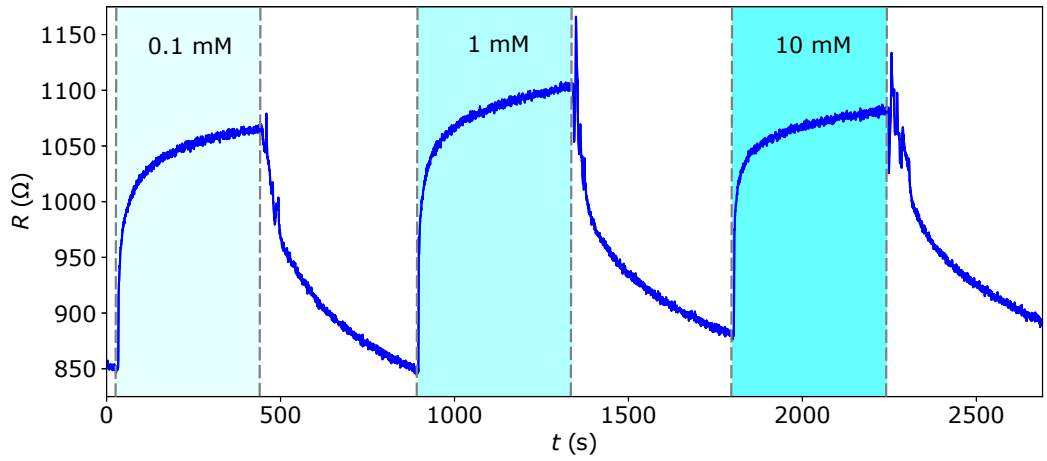

Fig. 6.1: Reaction in time to the addition of different concentrations of adenosine (A-N).

The measured time response to adenine (A) and deoxyadenosine monophosphate (dAMP) has the same character as for adenosine (A-N), the relative change of resistance in response to the different concentrations of the substances is summarized in

Tab. 6.1: Relative change of resistance ΔR (%) after addition of different concentrations of A, A-N, dAMP, and a reference measurement for the aqueous solution.

substance \ c (mM)	0.1	1	10
A	12.9 %	17.2 %	9.1 %
A-N	25.3 %	29.9 %	22.8 %
dAMP	31.1 %	34.1 %	22.4 %
H_2O	8.3 %		

Tab. 6.1. The change is calculated as the difference between the maximal value of resistance $R_{\max}$ before the removal of the droplet and the value of initial resistance R_0 stabilized before the addition of the droplet:

$$\Delta R = \frac{R_{\max} - R_0}{R_0}, \tag{6.1}$$

both values are averaged over 5 s time period. A reference measurement is done with a sample of the aqueous solution that the substances are diluted in.

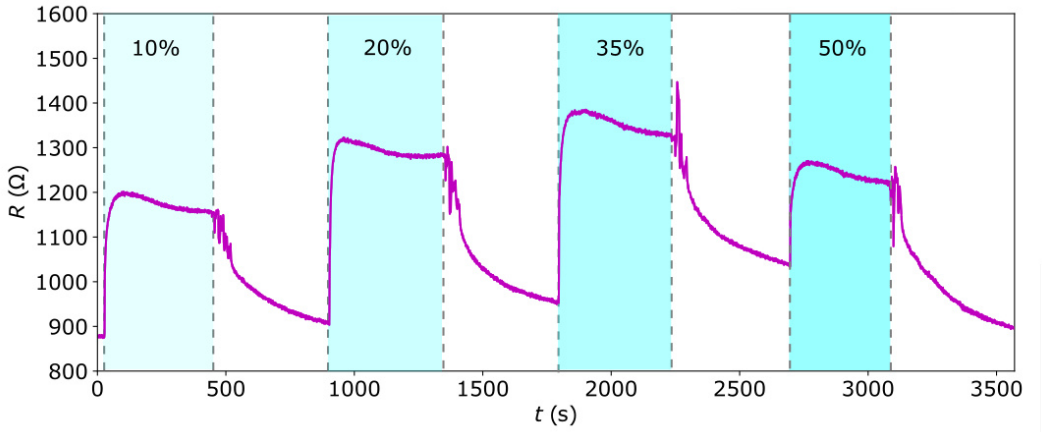

Fig. 6.2: Reaction in time to the addition of different concentrations of urea.

The reaction to the addition of urea (Fig. 6.2) follows a similar pattern: first an immediate increase of resistance and then a gradual stabilization with time. However, in this case, resistance decreases during the stabilization period. Tab. 6.2 contains the relative change (calculated by eq. 6.1) for the measured concentrations and a reference measurement of DI water.

Tab. 6.2: Relative change of resistance ΔR (%) after addition of different concentrations of urea and a reference measurement of DI water.

substance \ c (%)	10	20	35	50
urea	36.7 %	44.6 %	46.9 %	24.3 %
DI water	17.4 %			

6.2 Transfer curve measurements

The peak of the transfer curve corresponds to the Dirac point voltage V_{D}, where the Fermi level intersects the Dirac point. The type and degree of doping of graphene

caused by the adsorption of atoms or molecules can be determined based on the shift of V_D.

Fig. 6.3 shows a typical measurement of the transfer curve using the electrolytic top gate: for the 50 % solution of urea, the gate voltage is swept 0 V $\rightarrow$ 0.5 V $\rightarrow$ -1 V $\rightarrow$ 0 V with 0.01 V/0.5 s step and a noticeable hysteresis is observed. Resistance decreases when the sweeping gate voltage V_G moves away from the Dirac point voltage V_D and increases when the V_G sweeps close to the V_D again. This corresponds to the movement of the Fermi level away and then back closer to the Dirac point. The voltage range is adjusted for the reference measurement of DI water to better capture the peak of the transfer curve. The higher values of resistance in the reference measurement are mainly caused by the degradation of graphene with the use of the sensor.

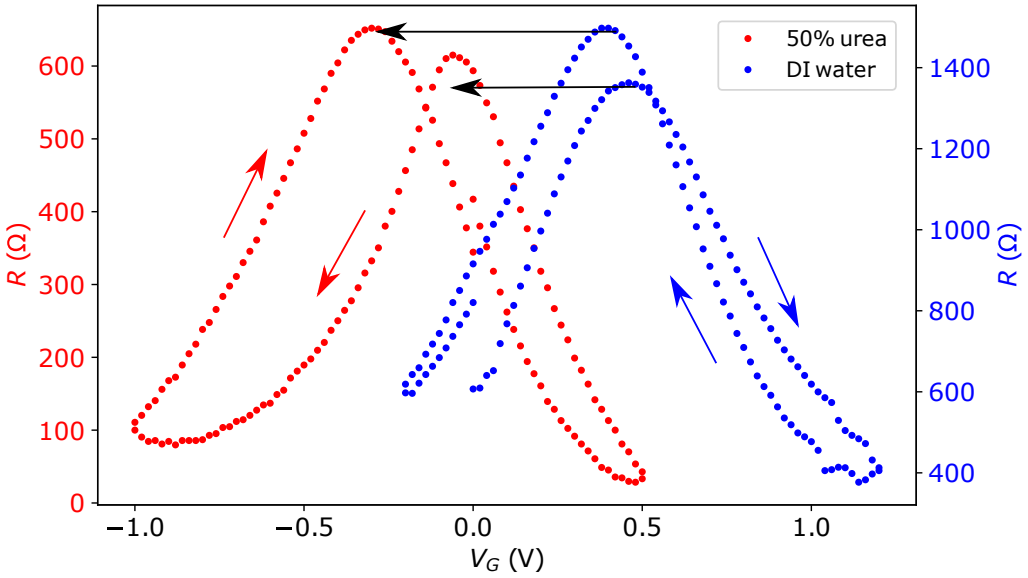

Fig. 6.3: Comparison of transfer curves for urea and DI water. Coloured arrows point in the direction of the voltage sweep. Black arrows mark the shift of both peaks from the reference measurement of DI water to the measurement of the urea solution.

In the majority of measurements, the right peak was better defined than the left one. For this reason, the position of the right peak is examined in the results analysis of the transfer curves.

For the adenine-based samples, seven measurements were done with the use of the electrolytic top gate and four with the solid bottom gate. The results are shown in Fig. 6.4. The graphs plot the position of the Dirac point voltage V_D depending on the concentration for each of the samples. Reference measurements of the aqueous

solution found $V_D = (0.21 \pm 0.08)\,V$ with the top gate and $V_D = (12 \pm 3)\,V$ with the bottom gate.

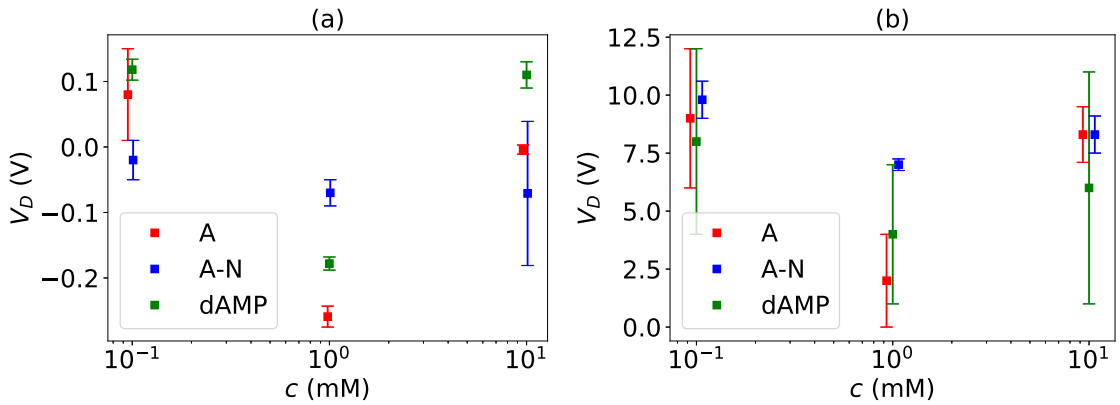

Fig. 6.4: Position of the Dirac point voltage V_D for adenine-based substances using the electrolytic top gate (a) and the solid-state bottom gate (b). Data points were moved fractionally along the x-axis for clarity.

The different concentrations of urea were measured five times with top gating and four times with bottom gating, Fig. 6.5. Reference measurements done for DI water determined the Dirac point voltage as $V_D = (0.46 \pm 0.06)\,V$ with the top gate and $V_D = (25 \pm 2)\,V$ with the bottom gate.

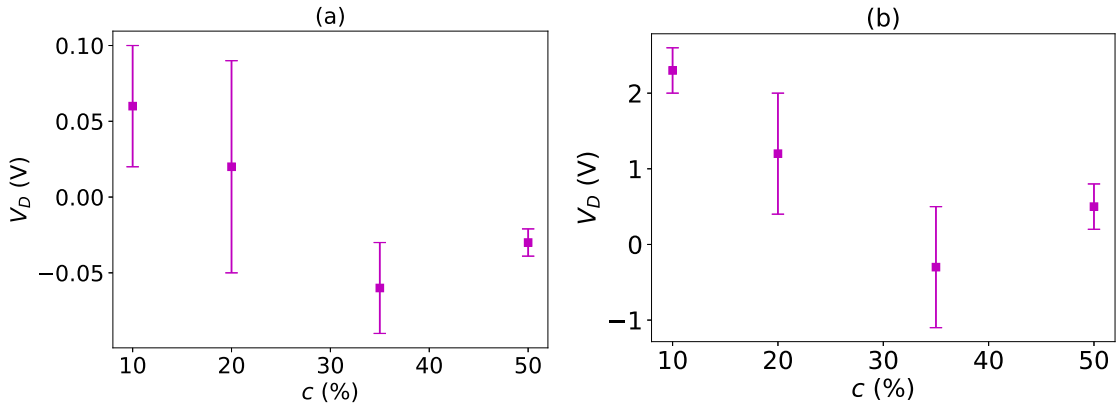

Fig. 6.5: Results of urea with the electrolytic top gate (a) and the solid-state bottom gate (b).

The concentration of majority carriers in graphene can be calculated using the model of a parallel-plate capacitor, as described in section 2.1. Substituting gate voltage V_G in eq. 2.4 with the Dirac point voltage V_D measured for the individual substances by the solid-state bottom gate gives the concentration of majority carriers in graphene with the adsorbed molecules, Fig. 6.6.

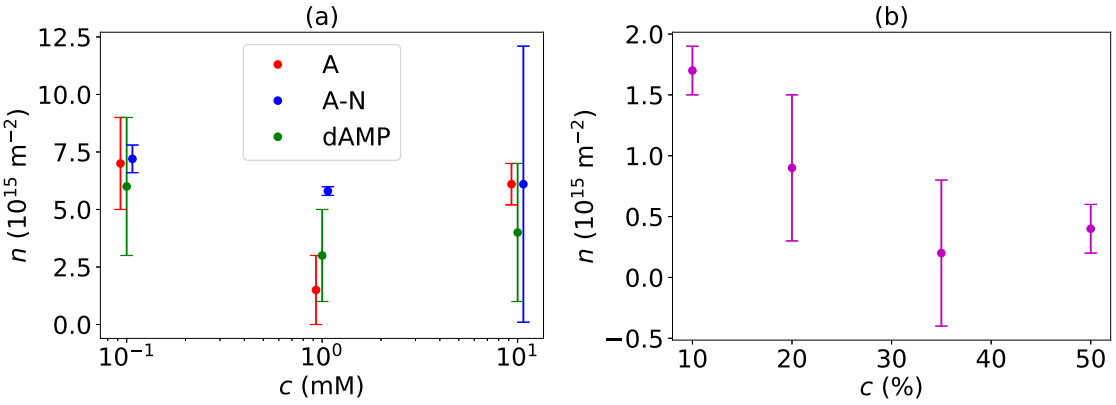

Fig. 6.6: Concentration of the majority carriers as calculated by eq. 2.4 from the solid-state bottom gate measurements for adenine-based samples (a) and urea (b).

6.3 Discussion

Based on the results obtained from transfer curve measurements, all adenine-based samples cause n-doping of graphene. The peak shifts to the left compared to the reference measurements of the aqueous solution and the Dirac point voltage V_D moves into low values of the gate voltage V_G. Experiments done in atmospheric conditions show that all graphene sensors are originally heavily p-doped.

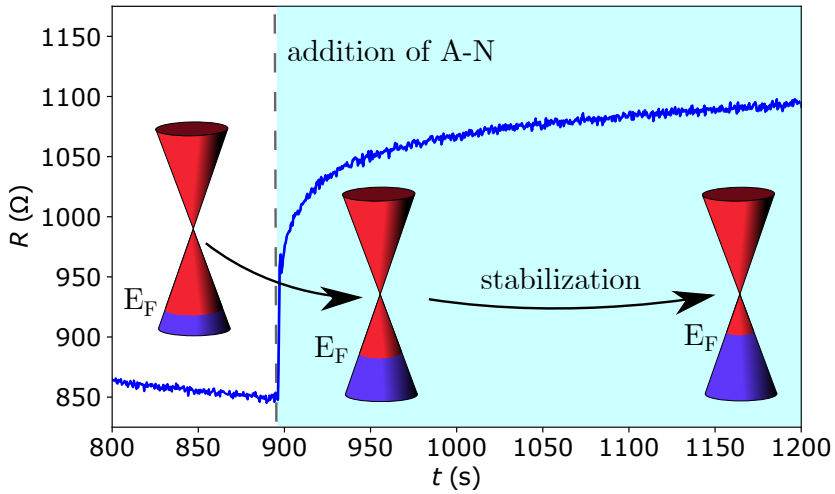

Fig. 6.7: The movement of the Fermi level after the addition of 1 mM A-N.

This conclusion is further supported by the time response measurements, where the immediate reaction is an increase of resistance, meaning that the Fermi level moves closer to the Dirac point and graphene accepts electrons, Fig. 6.7.

The results for adenine (A) are in agreement with results obtained both experimentally [20] and by DFT calculations of adsorption of nucleobases on graphene [17, 19]. However, both studies predict only negligible charge transfer of $0.02-0.03\,\mathrm{e}$ from the individual nucleobases to graphene. Adsorption of adenosine (A-N) was measured experimentally [21] with the resulting shift of the transfer curve found also to the left compared to pristine graphene. No experimental or theoretical studies were found for the adsorption of nucleotides (such as dAMP) on graphene. The adenine nucleobase at the core of the dAMP nucleotide causes n-doping, while the negatively charged phosphate group induces p-doping and predictions about the overall effect are difficult to make without previous calculations examining the strength of these opposing effects.

Additionally, the transfer curve measurements show that doping becomes stronger with increasing concentration (as demonstrated by the further shift of V_D for the 1 mM concentrations compared to the shift of V_D for the 0.1 mM concentrations), but the opposite tendency is observed for high concentrations. The same effect is observed in the time response measurements for different concentrations, Tab. 6.1. A possible explanation might be that at a sufficiently high concentration the molecules begin interacting between themselves forming weak bonds. The formation of these bonds consumes electrons that are taken back from graphene, lowering its Fermi level.

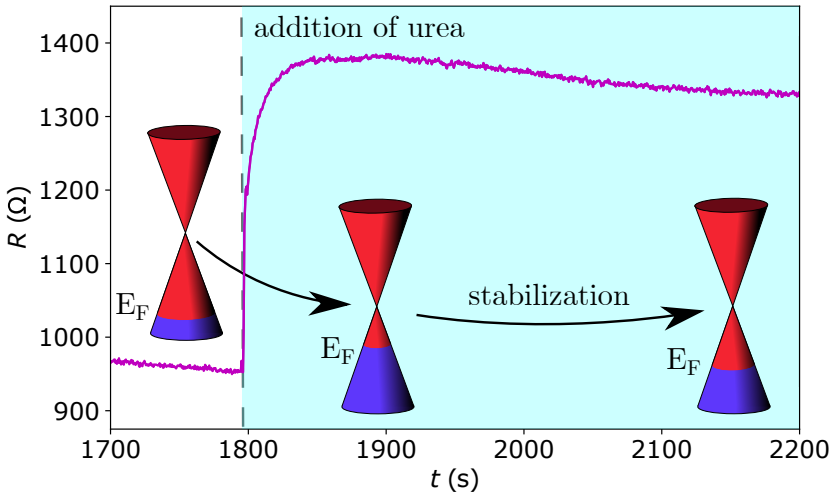

Fig. 6.8: The movement of the Fermi level after the addition of 35 % urea.

The same behavior can be seen in the results of transfer curve measurements for different concentrations of urea and identical reasoning may be applied. Based on these measurements, adsorbed urea induces n-doping of graphene. This result runs

contrary to a theoretical study done by DFT [22], which predicts only a very small p-doping of graphene with a charge transfer of 0.065 e.

The initial time response to the addition of urea supports n-doping as in the case with the adenine-based samples. However, during the stabilization period, resistance decreases, opposite to the stabilization of the adenine-based samples. This discrepancy can be explained by the observed hysteresis, when the Dirac point can "drift" with time. The transfer curve measurements show the Dirac point voltage V_{D} very close to 0 V for both top and bottom gating, much closer than for any of the adenine-based samples. In the majority of these measurements for urea with the solid-state bottom gate, the second peak appears to the right of the first one, indicating that the V_{D} drifts to the right with time and the resistance should decrease in response, Fig. 6.8. Measuring the time response without gating, i.e., at $V_{\mathrm{G}} = 0$ V and therefore very close to the V_{D}, could make this drifting more pronounced.

Conclusion

The aim of this thesis was to detect biochemichal substances using a graphene sensor. For this purpose, two designs of sensors were fabricated and two types of experiments were performed. Urea, adenine, adenosine, and deoxyadenosine monophosphate were chosen as samples of the biochemical substances.

The first experiment examined change in the resistance after the addition of the measured sample as a function of time. The second experiment obtained the transfer curve of graphene and the doping effects caused by the adsorption of the samples. This was done by applying gate voltage on either the electrolytic top gate, or the solid-state bottom gate and measuring the resistance of graphene.

Both types of experiments confirmed that the samples based on nucleic acids cause n-doping of graphene, in accordance with results reported in literature. Adsorbed urea also induces n-doping, however, DFT calculations suggest that only negligible p-doping should occur.

In all experiments was observed a dependency of doping on the concentration of the measured sample. At first, doping of graphene increases with rise in concentration, but the opposite effect is observed at high concentrations. A proposed explanation is that at sufficiently high concentrations, the individual molecules begin interacting between themselves forming weak bonds. The formation of these bonds consumes electrons that are taken back from graphene, moving the Fermi level in the process.

Due to the use of liquid samples in the measurements, a significant hysteresis was observed, suggesting that the Dirac point of graphene "drifts" in time after the addition of the measured sample. This effect should be taken under consideration, especially in measurements with longer duration, as it can alter the sensor response.

Further research based on the work done in this thesis should be directed at the functionalization of graphene, which is a necessary requirement for future applications in sensing and detection using graphene-based sensors. Additionally, a third type of measurement using the Hall effect could be designed to directly measure the concentration of majority carriers.

Bibliography

[1] NOVOSELOV, K. S., A. K. GEIM, S. V. MOROZOV, D. JIANG, Y. ZHANG, S. V. DUBONOS, I. V. GRIGORIEVA a A. A. FIRSOV. Electric Field Effect in Atomically Thin Carbon Films. *Science*. 2004, **306**(5696), 666-669. ISSN 0036-8075. doi: 10.1126/science.1102896

[2] LEE, C., X. WEI, J. W. KYSAR, J. HONE a J. MARROW. Measurement of the Elastic Properties and Intrinsic Strength of Monolayer Graphene. *Science*. 2008, **321**(5887), 385-388. ISSN 0036-8075. doi: 10.1126/science.1157996

[3] BALANDIN, Alexander A., Suchismita GHOSH, Wenzhong BAO, Irene CALIZO, Desalegne TEWELDEBRHAN, Feng MIAO a Chun Ning LAU. Superior Thermal Conductivity of Single-Layer Graphene. *Nano Letters*. 2008, **8**(3), 902-907. ISSN 1530-6984. doi: 10.1021/nl0731872

[4] NAIR, R. R., P. BLAKE, A. N. GRIGORENKO, K. S. NOVOSELOV, T. J. BOOTH, T. STAUBER, N. M. R. PERES a A. K. GEIM. Fine Structure Constant Defines Visual Transparency of Graphene. *Science*. 2008, **320**(5881), 1308-1308. ISSN 0036-8075. doi: 10.1126/science.1156965

[5] BUNCH, J. Scott, Scott S. VERBRIDGE, Jonathan S. ALDEN, Arend M. VAN DER ZANDE, Jeevak M. PARPIA, Harold G. CRAIGHEAD a Paul L. MCEUEN. Impermeable Atomic Membranes from Graphene Sheets. *Nano Letters*. 2008, **8**(8), 2458-2462. ISSN 1530-6984. doi: 10.1021/nl801457b

[6] CASTRO NETO, A. H., F. GUINEA, N. M. R. PERES, K. S. NOVOSELOV a A. K. GEIM. The electronic properties of graphene. *Reviews of Modern Physics*. 2009, **81**(1), 109-162. ISSN 0034-6861. doi: 10.1103/RevModPhys.81.109

[7] RUAN, Gedeng, Zhengzong SUN, Zhiwei PENG a James M. TOUR. Growth of Graphene from Food, Insects, and Waste. *ACS Nano*. 2011, **5**(9), 7601-7607. ISSN 1936-0851. doi: 10.1021/nn202625c

[8] ANDRONESCU, Corina a Wolfgang SCHUHMANN. Graphene-based field effect transistors as biosensors. *Current Opinion in Electrochemistry*. 2017, **3**(1), 11-17. ISSN 24519103. doi: 10.1016/j.coelec.2017.03.002

[9] SCHEDIN, F., A. K. GEIM, S. V. MOROZOV, E. W. HILL, P. BLAKE, M. I. KATSNELSON a K. S. NOVOSELOV. Detection of individual gas molecules adsorbed on graphene. *Nature Materials*. 2007, **6**(9), 652-655. ISSN 1476-1122. doi: 10.1038/nmat1967

[10] HWANG, Michael Taeyoung, Mohammad HEIRANIAN, Yerim KIM, et al. Ultrasensitive detection of nucleic acids using deformed graphene channel field effect biosensors. *Nature Communications*. 2020, **11**(1), 1543. ISSN 2041-1723. doi: 10.1038/s41467-020-15330-9

[11] LINDVALL, Niclas. *Towards graphene-based devices: Fabrication and characterization*. Gothenburg, Sweden, 2012. Doctoral Thesis. Chalmers University of Technology.

[12] Calculating the Capacitance. HALLIDAY, David, Robert RESNICK a Jearl WALKER. *Fundamentals of Physics*. 9th ed. Hoboken, USA: Wiley, 2011, s. 659-660. ISBN 978-0-470-46908-8.

[13] WU, Guangfu, Xin TANG, Zihong LIN, Meyya MEYYAPPAN a King Wai Chiu LAI. The effect of ionic strength on the sensing performance of liquid-gated biosensors. *2017 IEEE 17th International Conference on Nanotechnology (IEEE-NANO)*. IEEE, 2017, 2017, 242-245. ISBN 978-1-5090-3028-6. doi: 10.1109/NANO.2017.8117313

[14] HUNTER, Christopher A. a Jeremy K. M. SANDERS. The nature of .pi.-.pi. interactions. *Journal of the American Chemical Society*. 1990, **112**(14), 5525-5534. ISSN 0002-7863. doi: 10.1021/ja00170a016

[15] ZARUDNEV, Eugene, Stepan STEPANIAN, Ludwik ADAMOWICZ a Victor KARACHEVTSEV. Noncovalent Interaction of Graphene with Heterocyclic Compounds: Benzene, Imidazole, Tetracene, and Imidazophenazines. *ChemPhysChem*. 2016, **17**(8), 1204-1212. ISSN 14394235. doi: 10.1002/cphc.201500839

[16] The Chemistry and Function of Nucleic Acids. BEYER, Hans a Wolfgang WALTER. *Organic Chemistry: A Comprehensive Degree Text and Source Book.* 22nd ed. Chichester, England: Albion Publishing Limited, 1997, p. 849-856. ISBN 978-1-898563-37-2.

[17] GOWTHAM, S., Ralph H. SCHEICHER, Rajeev AHUJA, Ravindra PANDEY a Shashi P. KARNA. Physisorption of nucleobases on graphene: Density-functional calculations. *Physical Review B*. 2007, **76**(3). ISSN 1098-0121. doi: 10.1103/PhysRevB.76.033401

[18] LE, Duy, Abdelkader KARA, Elsebeth SCHRÖDER, Per HYLDGAARD a Talat S RAHMAN. Physisorption of nucleobases on graphene: a comparative van der Waals study. *Journal of Physics: Condensed Matter*. 2012, **24**(42). ISSN 0953-8984. doi: 10.1088/0953-8984/24/42/424210

[19] LEE, Jun-Ho, Yun-Ki CHOI, Hyun-Jung KIM, Ralph H. SCHEICHER a Jun-Hyung CHO. Physisorption of DNA Nucleobases on h -BN and Graphene: vdW-Corrected DFT Calculations. *The Journal of Physical Chemistry C*. 2013, **117**(26), 13435-13441. ISSN 1932-7447. doi: 10.1021/jp402403f

[20] DONTSCHUK, Nikolai, Alastair STACEY, Anton TADICH, et al. A graphene field-effect transistor as a molecule-specific probe of DNA nucleobases. *Nature Communications*. 2015, **6**(1). ISSN 2041-1723. doi: 10.1038/ncomms7563

[21] LIN, Cheng-Te, Phan Thi Kim LOAN, Tzu-Yin CHEN, Keng-Ku LIU, Chang-Hsiao CHEN, Kung-Hwa WEI a Lain-Jong LI. Label-Free Electrical Detection of DNA Hybridization on Graphene using Hall Effect Measurements: Revisiting the Sensing Mechanism. *Advanced Functional Materials*. 2013, **23**(18), 2301-2307. ISSN 1616301X. doi: 10.1002/adfm.201202672

[22] SINGH, Rajan a Roy PAILY. Adsorption of Urea over Transition Metal-Doped Graphene: A DFT Study. *Journal of Electronic Materials*. 2019, **48**(11), 6940-6948. ISSN 0361-5235. doi: 10.1007/s11664-019-07573-0

[23] PIASTEK, Jakub *Příprava grafénových vrstev pokrytých Ga atomy a charakterizace jejich elektrických vlastností.* Brno, 2015. Master's Thesis. Brno University of Technology, Faculty of Mechanical Engineering, Institute of Physical Engineering.

[24] TRIPSKÝ, Andrej. *Design, fabrication and testing of graphene biosensors.* Brno, 2020. Master's Thesis. Brno University of Technology, Faculty of Mechanical Engineering, Institute of Physical Engineering.

[25] BARTOŠÍK, Miroslav, Jindřich MACH, Jakub PIASTEK, David NEZVAL, Martin KONEČNÝ, Vojtěch ŠVARC, Klaus ENSSLIN a Tomáš ŠIKOLA. Mechanism and Suppression of Physisorbed-Water-Caused Hysteresis in Graphene FET Sensors. *ACS Sensors*. 2020, **5**(9), 2940-2949. ISSN 2379-3694. doi: 10.1021/acssensors.0c01441

List of symbols, quantities and abbreviations

A	adenine
A-N	adenosine
CEITEC	Central European Institute of Technology
CVD	chemical vapour deposition
dAMP	deoxyadenosine monophosphate
DFT	density functional theory
DI	deionized (water)
DNA	deoxyribonucleic acid
DOS	density of states
EBPVD	electron-beam physical vapour deposition
EDL	electric double layer
$\mathbf{Fe(NO_3)_3 \cdot 9\,H_2O}$	iron(III) nitrate nonahydrate
FET	field-effect transistor
GFET	graphene field-effect transistor
LOD	limit of detection
PMMA	poly(methyl methacrylate)
PVD	physical vapour deposition
RF	radio frequency
RIE	reactive-ion etching
RNA	ribonucleic acid
$\mathbf{SiO_2}$	silicon dioxide
UHV	ultra high vacuum
UV	ultra-violet
E_F	Fermi level

λ_{D}	Debye length
V_{D}	Dirac point voltage
V_{G}	gate voltage